# *In-vitro* and *in-vivo* analyses of the effects of source, length, and charge on the cytotoxicity and immunocompatibility of cellulose nanocrystals

Adam M. Weiss<sup>1,2</sup>, Nicholas Macke<sup>2</sup>, Yefei Zhang<sup>2</sup>, Celine Calvino<sup>2</sup>, Aaron P. Esser-Kahn,<sup>2,\*</sup> Stuart J. Rowan<sup>1,2,3,\*</sup>

<sup>&</sup>lt;sup>1</sup> Department of Chemistry, University of Chicago 5735 S Ellis Ave., Chicago, IL 60637, United States

<sup>&</sup>lt;sup>2</sup> Pritzker School of Molecular Engineering, University of Chicago 5640 S. Ellis Ave., Chicago, IL 60637, USA

<sup>&</sup>lt;sup>3</sup> Chemical and Engineering Sciences, Argonne National Laboratory 9700 Cass Avenue, Lemont, Illinois 60439, United States

<sup>\*</sup> Corresponding authors E-mail: stuartrowan@uchicago.edu, aesserkahn@uchicago.edu

#### Abstract

Cellulose nanocrystals (CNCs) are an emergent, sustainable nanomaterial which are bio-sourced, abundant, and biodegradable. On account of their high aspect ratio, low density, and mechanical rigidity, they have been employed in numerous areas of biomedical research including as reinforcing materials for bone or tissue scaffolds or as carriers in drug delivery systems. Given the promise of these materials for such use, characterizing and understanding their interactions with biological systems is an important step to prevent toxicity or inflammation. Reported herein are studies aimed at exploring the *in-vitro* and *in-vivo* effects that source, length, and charge of the CNCs have on cytotoxicity and immune response. CNCs from four different biosources (cotton, wood, Miscanthus x. Giganteus, and sea tunicate) were prepared and functionalized with positive or negative charges to obtain a small library of CNCs with a range of dimensions and surface charge. A method to remove endotoxic or other impurities on the CNC surface leftover from the isolation process was developed, and the biocompatibility of the CNCs was subsequently assayed *in-vitro* and *in-vivo*. After subcutaneous injection, it was found that unfunctionalized (uncharged) CNCs form aggregates at the site of injection, inducing splenomegaly and neutrophil infiltration, while charged CNCs having surface carboxylates, sulfate half-esters, or primary amines were biologically inert. No effect of particle source or length was observed in the *in-vitro* and *in-vivo* studies conducted. The lack of *in-vitro* or *in-vivo* immune response toward charged CNCs in these experiments supports their use in future biological studies.

# **Keywords**

Cellulose nanocrystals, biomaterials, tissue scaffolds, nanomedicine, biocompatibility

# Introduction

Cellulose nanocrystals (CNCs) have emerged as a green nanomaterial with properties that are desirable for a wide range of applications in polymer and materials science. Cellulose is a  $\beta(1\rightarrow 4)$ -linked D-glucose polymer which is predominantly found in the cell walls of plants, providing mechanical reinforcement by forming an ordered, hierarchical structure. This naturally occurring biostructure can be broken down using a series of base, bleach, and acid washes (aided by mechanical agitation) to obtain crystalline nanorods called cellulose nanocrystals, thereby offering a route to a green, abundant, and relatively low-cost source of organic nanomaterials.<sup>1</sup> Depending on the biological source and conditions used during the isolation process, CNCs with a wide range of lengths (50-5,000 nm) and aspect ratios (1-100) can be obtained. <sup>1-3</sup> The resulting crystalline materials are biodegradable and have a property profile that includes low density, mechanical rigidity, and optical transparency when homogenously dispersed in a host matrix. 1, 4, 5 CNCs can also be chemically modified to allow tuning of their properties. <sup>1, 6, 7</sup> CNCs have been investigated in a diverse range of applications from packaging and materials reinforcement to optoelectronic and water purification systems, among others.<sup>1, 7</sup> As such, the annual number of patents filed involving CNCs has increased more than seven-fold between 2013 and 2017, a trend that is expected to continue in the future with increased availability of and interest in CNCs.8

Beyond their use in materials engineering applications, CNCs have gained attention as an attractive nanomaterial for biomedicine, owing to their unique physicochemical properties, ease of isolation and functionalization, and abundance in nature. Early studies have shown applications for CNC-based composites in biomaterial scaffolds, antimicrobial dressings, and bioimaging devices. For example, poly(vinyl acetate)-CNC composites have been investigated as mechanically adaptable intracortical probes that display enhanced mechanical compliance

between the probes and neural tissue, thereby reducing inflammation and scarring relative to more traditional stiffer silicon-based probes. <sup>16-18</sup> CNCs have also found use in the delivery of small molecules, proteins, and nucleic acids, which can be attached to the CNCs through covalent and non-covalent bonds or delivered using CNCs in hydrogels or micellar formulations. <sup>20-28</sup> Notably, De France and colleagues report that CNC-PEG conjugates can adsorb proteins and be injected to form a hydrogel *in-situ*, remaining at the site of injection for months to allow site-specific release of cargo. <sup>26</sup> With the increased interest in and availability of CNCs, it is imperative to address how CNCs interact with biological systems to ensure safe implementation.

To date, studies that have addressed the biocompatibility of CNCs have been limited predominantly to in-vitro or respiratory uptake models. Nanoscale materials often interact with cells and tissues differently than bulk material owing to their high surface area to volume ratios and presence of positive or negative surface charges, which can affect cellular uptake, chemical adsorption, and pharmacological clearance of the materials.<sup>29</sup> In particular, high aspect ratio nanoparticles such as carbon nanotubes<sup>30, 31</sup> and fibrous silica<sup>32</sup> have been the subject of significant concern on account of early reports of pulmonary and cellular toxicity. Indeed, testing on CNCs has indicated that they can exhibit asbestos-like pulmonary toxicity in a murine respiratory uptake model owing to their low density, nanoscale properties, and surface chemistry.<sup>33</sup> It is interesting to note that in these studies and related model pulmonary studies the aspect ratio of the CNCs<sup>34</sup> or whether the CNCs were in an aqueous suspension or powder form<sup>33</sup> does impact the nature of the biological response. While there is still a lot to learn and understand about the potential pulmonary toxicity of CNCs, CNCs differ from carbon nanotubes because they are dispersible in water, potentially allowing for safer handling as aqueous slurries or dispersions. Dispersed wood-derived CNCs have been shown *in-vitro* to have no disruptive effect on cell viability on multiple cell lines at biologically relevant concentrations of < 250  $\mu g/mL$ ,  $^{35}$  potentially opening the door to aqueous CNC solutions and their derivatives being investigated in further diagnostic and therapeutic medical devices and drug delivery systems.

Although these results suggest the *in-vitro* biocompatibility of CNCs, they do not address the effects of functionalization, particle shape, or isolation procedures of CNCs in-vitro or in-vivo. For example, surface charge modification has been shown to alter cellular interactions with CNCs both *in-vitro* and in a zebrafish model. 36-38 Mahmoud *et al.* report that functionalizing CNCs with a positive (RBITC) or negative (FITC) charged fluorophore altered cellular uptake in-vitro using HEK and Sf9 cell lines.<sup>36</sup> Particle size was also shown to alter respiratory clearance of CNCs, as CNCs sourced from tunicate ( $l = 2,244\pm1,687$  nm) invoked greater respiratory inflammation than those sourced from cotton ( $l = 237 \pm 118$  nm). <sup>34</sup> Finally, chemical agents or bacterial contamination encountered during the isolation and functionalization process can also confound biological studies if incompletely removed. Labet and Thielemans reported that cleaning CNCs by Soxhlet extraction enhances reproducibility of functionalization reactions, highlighting the importance of removing debris from the surface of CNCs.<sup>39</sup> With increased interest in the commercial production of CNCs using different sources and isolation procedures, the work reported herein is aimed to more thoroughly examine how parameters, such as charge, length, and cleaning procedures of the CNC surface, impact *in-vitro* and *in-vivo* cytotoxicity and immunocompatibility incurred by the various CNCs. While Colombo et al. previously evaluated the in-vivo tissue distribution of subcutaneously injected AF647-modified CNCs, 40 this is the first study to our knowledge which evaluates the effects of CNC source on biocompatibility and the first which evaluates the in-vivo effects of source and charge after subcutaneous injection. A comprehensive review of *in-vitro* and *in-vivo* biocompatibility studies on cellulose-based materials were recently published by Ventura et al.<sup>41</sup>

To evaluate the effects of CNCs with different sizes and dimensions, CNCs from four different biosources including wood (w-), cotton (c-), Miscanthus x. Giganteus (MxG-), and tunicate (t-) were targeted for investigation. In addition, CNCs with different surface chemistry affording a variety of charges were targeted (Figure 1). Finally, CNCs produced via large scale production (ls) were compared to those produced on a smaller laboratory scale in order to evaluate whether the method of production would alter the biological response. A total of twelve different CNCs were studied. Uncharged CNCs (MxG-CNC-OH, obtained via hydrochloric acid hydrolysis) and CNCs functionalized with sulfate half-esters (c-CNC-OSO<sub>3</sub>-, MxG-CNC-OSO<sub>3</sub>-, and t-CNC-OSO<sub>3</sub>-, obtained via sulfuric acid hydrolysis) were prepared directly from the biosource using literature procedures. 42-44 c-CNC-OSO<sub>3</sub>-, MxG-CNC-OH, and t-CNC-OSO<sub>3</sub>- were further functionalized to yield CNCs with carboxylic acids (CNC-COOH, via TEMPO-based oxidation of the C6 alcohol)<sup>45</sup> or amines (CNC-NH<sub>2</sub>, via reaction of epichlorohydrin and ammonia) on their surface.<sup>25</sup> While unfunctionalized CNCs have a slight negative charge, it was hoped that a distribution of charges above and below this baseline would afford a distribution of relevant charges for downstream biological applications of CNCs. Finally, CNCs isolated on a larger, commercially-viable scale from wood (via sulfuric acid hydrolysis, w-CNC-OSO<sub>3</sub>-(ls))<sup>46, 47</sup> and Miscanthus x. Giganteus (via hydrochloric acid hydrolysis, MxG-CNC-OH<sub>(ls)</sub>)<sup>48, 49</sup> were obtained to allow a comparative analysis of isolation procedure on the biocompatibility of CNCs.

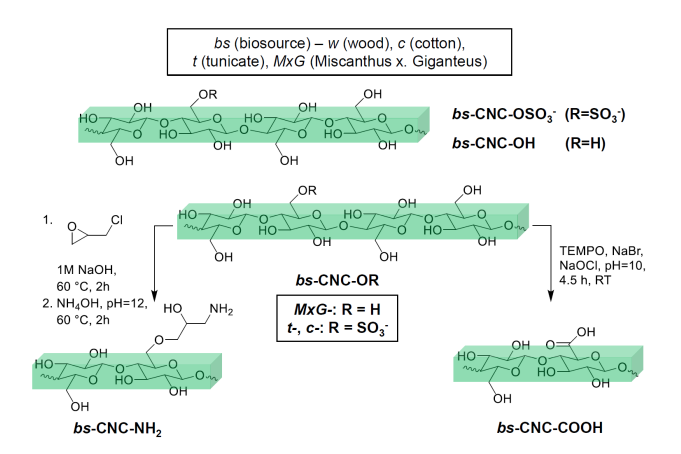


**Figure 1:** Overview of CNC synthesis. CNCs were obtained from tunicate, MxG, cotton, and wood to allow study of CNCs with four different lengths. CNCs were then functionalized using epichlorohydrin-mediated amination or TEMPO-oxidation to achieve CNCs with positive and negative charge modifications, respectively, on their surface.

# **Materials and Methods**

Materials and Mice. All chemicals unless otherwise noted were obtained from Sigma Aldrich and used without further purification. Sea tunicates (*Styela Clava*) were harvested from floating docks in Warwick Marina (Warwick, RI). Base-treated pulp from harvested *Miscantus x. Giganteus* was received as a generous gift from Aloterra Energy LLC (Conneaut, OH). Whatman Grade #1 filter paper and 2,2,6,6-Tetramethylpiperidine-1-oxyl (TEMPO) were obtained from Fisher Scientific. (±)-Epichlorohydrin was obtained from Alfa Aesar. Commercial scale *w*-CNC-OSO<sub>3</sub>-(*ls*) were purchased from Blue Goose Biorefineries Inc. (Saskatoon, SK),<sup>46,47</sup> and *MxG*-CNC-OH(*ls*) were received as a generous gift from the Materials Engineering Research Facility (MERF) at Argonne National Laboratory (Lemont, IL), who have developed a commercially scalable procedure for the isolation of CNCs from *Miscantus x. Giganteus*. <sup>48, 49</sup> RAW 264.7, RAW-Blue NF-κB reporter, and HEK-Blue mTLR4 reporter cells were obtained from InvivoGen. The cells were cultured in Dulbecco's Modified Eagle's Medium (DMEM) supplemented with 10% (v/v) fetal bovine serum (FBS), 100 U/mL penicillin, 100 μg/mL streptomycin, and selective antibiotics

and were maintained at 37 °C and 5% CO<sub>2</sub> atmosphere. All culture reagents were obtained from Thermo Fisher Scientific. For *in-vivo* experiments, six-week-old C57Bl/6J mice were obtained from Jackson Laboratories and acclimatized for 1 week prior to the onset of testing. Animals were housed under controlled light, temperature, and humidity conditions, supplied with food and water *ad libitum*, and monitored daily. All experiments were conducted with approval of the University of Chicago Institutional Animals Care and Use Committee, and animals were maintained in accordance with guidelines and regulations defined by the National Institutes of Health. Statistical analyses were performed using GraphPad Prism.

Isolation of Sulfated CNCs from Sea Tunicate Beak. Sea tunicates (Styela Clava) were cleaned and bleached following previously reported procedures.<sup>42</sup> Briefly, tunicates were gutted and their mantles collected. The mantles were washed in 5 wt.% aqueous potassium hydroxide at 80 °C for 8 h under continuous stirring. After rinsing with water, the mantles were washed again with potassium hydroxide solution at 80 °C for 16 h. The cleaned mantles were rinsed until the rinse pH was neutral. Bleaching was performed by adding the cleaned mantles (500 g) into 3 L of distilled water (dH<sub>2</sub>O) with 5 mL of glacial acetic acid and 10 mL of sodium hypochlorite (>4% chlorine). The temperature was increased to 60 °C and the mixture stirred for 1 h. Additional glacial acetic acid (5 mL) and sodium hypochlorite (10 mL) were added in 1 h intervals until the color of the mantles changed to white. Finally, the bleached tunicate mantles were rinsed with water and dried for further use. To hydrolyze the tunicate pulp and obtain crystalline CNCs, 5 g of dry bleached tunicate mantles were pulverized in 500 mL of dH<sub>2</sub>O using a kitchen blender to yield a fine cellulose pulp. 500 mL of sulfuric acid (98%) was then slowly added over 60 min with vigorous stirring to a suspension of the tunicate pulp in an ice bath. After the acid addition was completed, the reaction was heated to 60 °C and reacted for 1.5 h. The acid hydrolysis was quenched by adding 1 L of cold water to the reaction, and the suspension was then filtered through a fritted glass filter. The crude product was washed with  $dH_2O$  until pH > 6. It was re-dispersed in  $dH_2O$  at 1 wt.% by ultrasonication and dialyzed against  $dH_2O$  for 4 days. Finally, the hydrolyzed tunicate CNCs were recovered by lyophilization to obtain a white aerogel, t-CNC-OSO<sub>3</sub><sup>-</sup>.

Isolation of Sulfated and Unfunctionalized CNCs from *Miscanthus x Giganteus*. CNCs from *Miscanthus x. Giganteus* (MxG) were isolated from base-treated pulp using previously reported methods with minor changes. MxG pulp was reacted four times with 4.0 L of 2 wt.% sodium hydroxide solution, once at 25 °C and three times at 100 °C for 24 h, filtering and washing with dH<sub>2</sub>O after each step until the pH < 8. The resulting pulp was reacted twice with 4.0 L of 2 wt.% sodium hypochlorite (>4% chlorine) and 15 mL of glacial acetic acid for 2 h at 70 °C. The resulting solution was cooled, filtered, washed with dH<sub>2</sub>O, and freeze dried to yield 150 g of cellulose fiber as a white pulp. To isolate MxG-CNC-OH, the bleached white pulp was hydrolyzed with hydrochloric acid. 3.0 L of 1 M HCl was added to 100 g of the white MxG pulp and heated to 75 °C for 15 h. To obtain MxG-CNC-OSO<sub>3</sub>, the bleached white pulp was hydrolyzed with sulfuric acid. 250 mL of 30 wt.% H<sub>2</sub>SO<sub>4</sub> was added to 10 g of the MxG pulp and heated to 50 °C for 3 h. The resulting mixtures were cooled and filtered through a fritted glass filter. The filtered products were washed with dH<sub>2</sub>O until pH > 6, resuspended at 1 wt.%, dialyzed for 72 h against dH<sub>2</sub>O, and freeze-dried to yield CNCs (MxG-CNC-OH and MxG-CNC-OSO<sub>3</sub>) as white aerogels.

**Isolation of Sulfated CNCs from Cotton filter paper.** CNCs from Whatman #1 filter paper were isolated using previously reported methods with minor changes.<sup>44</sup> 5.2 g filter paper was initially suspended in 250 mL water and ground into an aqueous pulp using a kitchen blender. The pulp mixture was then placed in an ice bath, and 140 mL 98 wt.% sulfuric acid was added dropwise such that the temperature was held below 20 °C. After addition was complete, the ice

bath was removed and the mixture was reacted at 50 °C. After 3.5 h, the reaction was stopped by diluting the mixture with 3.0 L dH<sub>2</sub>O. The resulting suspension was filtered and washed using a fritted glass filter until the pH > 6.0. The product was resuspended in dH<sub>2</sub>O at 1 wt.%, dialyzed against dH<sub>2</sub>O for 72 h, and freeze-dried to yield cotton CNCs as a white aerogel, c-CNC-OSO<sub>3</sub><sup>-</sup>.

TEMPO Oxidation of CNCs. CNCs from tunicate, MxG, and cotton were treated with TEMPO to oxidize the C6 alcohol to a carboxylic acid. As an example, MxG-CNC-OH (4.14 g) was dispersed by sonication in 500 mL dH<sub>2</sub>O for 30 min. TEMPO (0.412 g) and NaBr (4.02 g) were then added and stirred until dissolved. Then, 10 wt.% of NaOCl (>4% chlorine) was added, and the mixture was stirred for 4.5 h at 25 °C in the dark while holding pH at 10–11 with 5 M NaOH. After the reaction was completed, NaCl (17.0 g) was added and stirred for 10 min. 2 M HCl was added to adjust the pH < 7, and the mixture was filtered through a fine-pore fritted glass filter to yield a crude solid. The solid was resuspended at 1 wt.% in dH<sub>2</sub>O and dialyzed against dH<sub>2</sub>O for 72 h. The dialyzed solution was freeze-dried to yield a white aerogel, MxG-CNC-COOH. This procedure was repeated using tunicate (t-CNC-OSO<sub>3</sub>-) and cotton CNCs (t-CNC-OSO<sub>3</sub>-) to obtain t-CNC-COOH and t-CNC-COOH, respectively.

Amine Functionalization of CNCs. CNCs from tunicate, MxG, and cotton were functionalized with amines using epichlorohydrin and ammonia according to a previously reported method.<sup>25</sup> As an example, MxG-CNC-OH (128 mg) was dispersed in 200 mL water by ultrasonication for 30 min. It was then reacted with epichlorohydrin (6 mmol/g CNC) at 60 °C for 2 h in the presence of 1 M NaOH to introduce an epoxy moiety to the surface of the CNCs. The product was dialyzed overnight until the pH was <12. The dialyzed product was then adjusted to pH of 12, and 1 mL of 29.4% aqueous NH<sub>4</sub>OH was added to the CNCs and reacted for 2 h at 60 °C to aminate the CNCs. The reaction was then cooled and filtered through a fine-pore fritted glass

filter. The crude product was dispersed by ultrasonication at 1 wt.% in dH<sub>2</sub>O, dialyzed against dH<sub>2</sub>O for 72 h, and freeze-dried to obtain a powdery white product, MxG-CNC-NH<sub>2</sub>. This procedure was repeated using sulfated tunicate (t-CNC-OSO<sub>3</sub><sup>-</sup>) and cotton CNCs (c-CNC-OSO<sub>3</sub><sup>-</sup>) to obtain t-CNC-NH<sub>2</sub> and c-CNC-NH<sub>2</sub>, respectively.

**Material Characterization.** Isolated and functionalized CNCs were characterized by FT-IR spectroscopy, electrophoretic light scattering (ELS), conductometric titration, and thermogravimetric analysis (TGA). Residual contamination was assessed by 400 MHz <sup>1</sup>H-NMR. All material characterization methods and results are available in the Supplementary Information.

Imaging. CNC-OSO<sub>3</sub>-, CNC-COOH, and CNC-NH<sub>2</sub> samples were imaged using atomic force microscopy (AFM). 0.01 wt.% of CNCs were dispersed by brief ultrasonication in dH<sub>2</sub>O and then prepared on an exfoliated mica substrate. The mica was coated with 50 μL poly-*L*-lysine for 2 min and then washed with dH<sub>2</sub>O. 50 μL of CNC solution was then loaded onto the mica and allowed to settle for 2 min before being washed with dH<sub>2</sub>O. Samples were dried overnight and imaged with a Cypher ES Environmental AFM (Asylum Research) using FS-1500 probes (Asylum Research). The length of CNCs was analyzed using height mode with Gwyddion for SPM (Czech Metrology Institute). On account of the low dispersibility of uncharged CNCs in water resulting in large aggregates during AFM imaging, *MxG*-CNC-OH<sub>(δ)</sub> and *MxG*-CNC-OH samples were instead imaged by transmission electron microscopy (TEM). For TEM imaging, 1.0 mg/mL CNC solutions were dispersed by brief ultrasonication in dH<sub>2</sub>O and then passed through a 10 μm pore-diameter filter to remove larger aggregates. About 10 μL of the filtered solution was drop cast on an ultrathin holey carbon-coated copper grid and stained with 2 wt.% uranyl acetate. The stained sample was immediately imaged using a FEI Technai F30 TEM (TSS Microscopy).

Wide Angle X-Ray Scattering. To assess crystallinity of CNC samples, Wide Angle X-ray Scattering (WAXS) was conducted on beamline 12-ID-B using the Advanced Photon Source at Argonne National Laboratory (Lemont, IL) with a Pilatus 300k detector (Dectris) or on a laboratory SAXSLAB GANESHA 300 XL system. On beamline 12-ID-B, samples were irradiated at a voltage of 13.3 KeV for 0.1 s. On the GANESHA system, samples were irradiated using a Cu K $\alpha$  source ( $\lambda$  = 0.154 nm) at a voltage of 40 kV for 30 min. CNCs were packed in a washer and held in place with Kapton tape. Samples were mounted in a vacuum chamber perpendicular to the collimated beam. Crystallinity Index was determined by the peak deconvolution method after subtracting the Kapton background, and peaks were fit in MATLAB to a Gaussian distribution function at the idealized diffraction peaks for cellulose 1 $\beta$  reported by A.D. French. 50, 51 Details on the fit function employed are described at depth in the Supplementary Information.

HEK mTLR4 Assay. HEK mTLR4 cells are used as a semiquantitative readout of endotoxin contamination. <sup>52</sup> CNCs were first washed 3 times with endotoxin-free water. For each wash, CNCs samples were dispersed at approximately 1,000 μg/mL in water, ultrasonicated for 5 min (3 s on/off cycles at 25% power), and subjected to ultracentrifugation at 10,000 G to precipitate the CNCs. The solutions were decanted and re-dispersed after each wash and freeze-dried at the end of cleaning. CNC concentrations of 10-100 μg/mL were then used to determine contamination of CNC samples. Particle suspensions of 100 and 1,000 μg/mL were prepared in endotoxin-free water, and 20 μL of each suspension was plated in triplicate in a 96 well plate. LPS-EK (InvivoGen) with a known endotoxin content was used as a positive control. HEK Blue detection media (InvivoGen) was reconstituted in 50 mL endotoxin-free water, heated to 37°C for 30 min, and passed through a 0.22 μm pore-diameter filter. HEK Blue mTLR4 cells were passaged and plated in the 96 well plate at 25,000 cells/well in 180 μL HEK Blue detection media. Cells were

incubated with the CNCs at 37 °C and 5% CO<sub>2</sub> overnight. The plate was analyzed after 12 h using a Multiskan FC plate reader (Thermo Scientific), and absorbance was measured at 620 nm.

MTT Assay. RAW-Blue cells were plated in a 96 well plate at 25,000 cells/well in 200  $\mu$ L DMEM containing 10% HI-FBS and selective antibiotics. Cells were incubated at 37 °C and 5% CO<sub>2</sub> for 24 h. Then, particle suspensions from 100 to 1,000  $\mu$ g/mL were prepared in endotoxin free water, diluted 1:10 in culture media, and added to the cells. 10% DMSO was used as a positive control. After 24 h, cell culture media was replaced with 50  $\mu$ L of 3-(4,5-dimethylthiazol-2-yl)-2,5-diphenyl tetrazolium bromide (MTT) reagent (1 mg/mL) and 50  $\mu$ L of FBS-free media. After incubation for 3 h, formazan crystals were dissolved in 150  $\mu$ L of a 10% w/v sodium dodecyl sulfate and 0.01 M HCl solution, protected from light, and incubated for 30 min. The absorbance was measured by a Multiskan FC plate reader (Thermo Scientific) at 590 nm.

**RAW-Blue NF-κB Assay.** RAW-Blue cells were passaged and plated in a 96 well plate at 25,000 cells/well in 200 μL DMEM containing 10% HI-FBS and selective antibiotics. Cells were incubated at 37 °C and 5% CO<sub>2</sub> for 24 h. Then, particle suspensions from 100 to 1,000 μg/mL were prepared in endotoxin-free water, diluted 1:10 in DMEM + 10% HI-FBS, and added to the cells. LPS-EK (InvivoGen) was used as a positive control. 24 h after the final addition, 20 μL of the cell supernatant was placed in 180 μL freshly prepared QuantiBlue (InvivoGen) solution and incubated at 37 °C and 5% CO<sub>2</sub> for up to 4 h. The plate was analyzed every hour using a Multiskan FC plate reader (Thermo Scientific) and absorbance was measured at 620 nm.

*In-vivo* biocompatibility experiment. To assay systemic inflammation incurred by the CNCs, CNCs were injected subcutaneously and assayed acute cytokine production, spleen mass, and inflammation at the site of injection. 0.1% or 0.5% CNC solutions were cleaned using the aforementioned procedure and dispersed in endotoxin-free water. To ensure that all CNCs were

injected at the same location, mice were anesthetized under 2-2.5% isoflurane and 2L/min oxygen flow. Mice were then injected in the left flank with the appropriate CNC solution (300 μL of 0.1% or 0.5% CNC/mouse, n=3-5/group). Mice were bled via facial vein 1 or 24 h after injection. Serum was isolated by ultracentrifugation, and cytokine production was analyzed using CBA Mouse Inflammation Cytokine Kit (BD Bioscience) according to the manufacturer's procedure. Flow cytometry was conducted using Novocyte flow cytometer (ACEA BioSciences), and data were processed in MATLAB and analyzed using GraphPad Prism. To assess tissue compatibility of the CNCs, mice were sacrificed after 2 or 30 d. The subcutaneous tissue was imaged and then collected for histological analysis. Spleens were also collected and weighed as a measure of systemic inflammation. Subcutaneous tissue was immediately fixed in 10% neutral buffered formalin for 36 h, dehydrated in ethanol, and embedded in paraffin. Tissues were sectioned with a microtome, stained with hematoxylin and eosin, and imaged using an Axio Observer 7 microscope (Carl Zeiss AG) with an Axiocam 506 color camera (Carl Zeiss AG). Based on the images, inflammatory response was assessed qualitatively with the assistance of a histopathologist.

#### **Results and Discussion**

**Isolation and functionalization of cellulose nanocrystals.** CNCs prepared from each of the four *in-house* procedures and those obtained from the two large scale isolation procedures were characterized by AFM or TEM, wide-angle X-ray scattering (WAXS), thermogravimetric analysis (TGA), and FT-IR to ensure no confounding factors would affect biocompatibility assessments. The length and morphology of the CNCs was evaluated using AFM, except in the case of the uncharged MxG-CNC-OH<sub>(ls)</sub> and MxG-CNC-OH samples which were imaged using TEM, as they disperse poorly in solution. As expected, tunicate-based CNCs (t-CNCs) were longest (820 $\pm$ 400

nm) (Figure 2A & Figure S1A), MxG-CNCs were shorter (190±60 nm and 120±40 nm for hydrochloric acid hydrolysis and sulfuric acid hydrolysis, respectively) (Figure 2B-C & Figure S1B-C), and cotton-based CNCs (c-CNCs) were shortest (90±20 nm) (Figure 2D & Figure S1D).<sup>4</sup> The MxG-CNC-OH<sub>(ls)</sub> samples (200±80 nm) were longer than MxG-CNC-OH prepared *in house* (Figure 2E & Figure S1E); which is possibly a consequence of differences in the length of acid treatment.<sup>2</sup> The w-CNC-OSO<sub>3</sub>-(ls) samples were 110±40 nm (Figure 2F & Figure S1F), which is commensurate with previous reports.

With the size of the isolated CNCs confirmed, WAXS, TGA, FT-IR, and conductometric titration experiments were subsequently conducted to evaluate the crystallinity index (CI) and chemical composition of the isolated CNCs. Using the peak deconvolution method for WAXS analysis (assuming a Gaussian distribution and modelling the cellulose 1β peaks of 101, 10ī, 021, and 002),<sup>50</sup> it was found that all CNCs were between 85-90% crystalline (Table 1 and Figures S2-S6). Through TGA (Figure S7), it was observed that all of the sulfated CNC samples had a lower degradation temperature than unfunctionalized *MxG*-CNC-OH and *MxG*-CNC-OH<sub>(ls)</sub>, which is consistent with previous reports.<sup>53</sup> FT-IR spectroscopy revealed no unexpected peaks or lignin contamination (which is observed as peaks at 1,604, 1,512 and 1,462 cm<sup>-1</sup> that correspond to the aromatic rings of lignin) in the samples (Figure S8).<sup>43</sup> Finally, conductometric titrations revealed the presence of about 170, 110, and 27 mmol/kg of sulfate half-ester groups on *t*-CNC-OSO<sub>3</sub>-, *MxG*-CNC-OSO<sub>3</sub>-, and *c*-CNC-OSO<sub>3</sub>-, respectively (Figure S9).

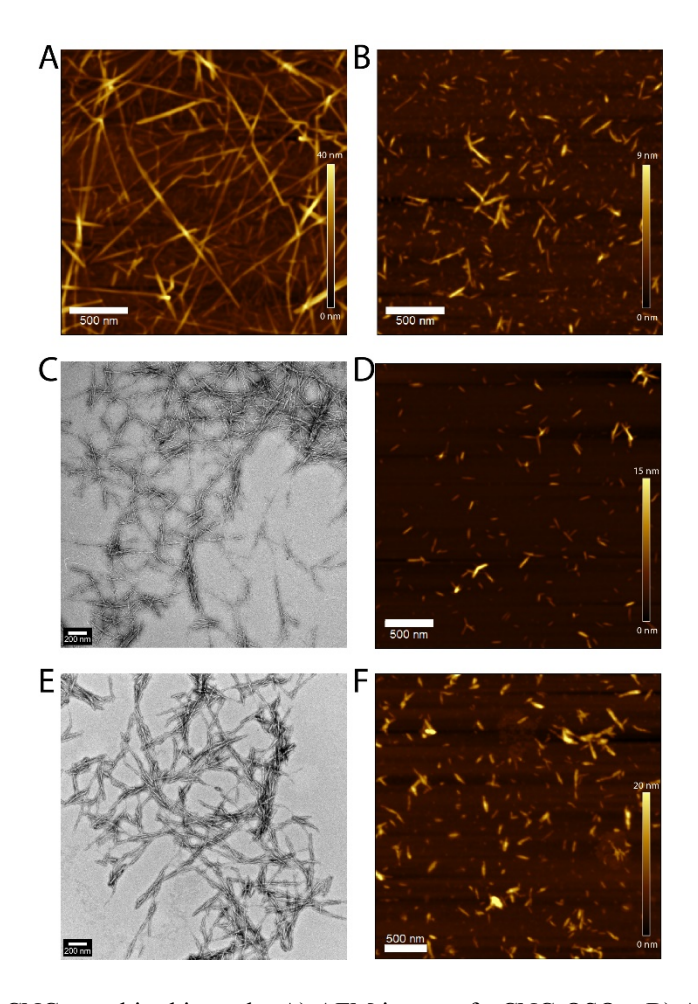


**Figure 2:** Microscopy of CNCs used in this study. A) AFM image of t-CNC-OSO<sub>3</sub><sup>-</sup>. B) AFM image of MxG-CNC-OSO<sub>3</sub><sup>-</sup>. C) TEM image of MxG-CNC-OH. D) AFM image of c-CNC-OSO<sub>3</sub><sup>-</sup>. E) TEM image of MxG-CNC-OH(ts). F) AFM image of w-CNC-OSO<sub>3</sub><sup>-</sup>(ts). For AFM imaging, samples were drop cast from a dilute aqueous solution onto a poly-lysine coated mica substrate, and for TEM imaging, samples were casted onto a carbon-coated copper grid and stained with uranyl acetate..

The isolated CNCs were subsequently modified to achieve a distribution of surface charges (Figure 1). *t*-CNC-OSO<sub>3</sub><sup>-</sup>, *MxG*-CNC-OH, and *c*-CNC-OSO<sub>3</sub><sup>-</sup> were TEMPO-oxidized to yield carboxylic acid-functionalized CNCs (CNC-COOH) or amine-functionalized (CNC-CNH<sub>2</sub> via epichlorohydrin-mediated amination) according to literature procedures and dialyzed for several days to remove impurities.<sup>25, 45</sup> The resulting chemically modified CNCs were characterized by

FT-IR (Figure S8), conductometric titration (Figure S9), and AFM (Figure S10), and their purity was assessed by semiquantitative <sup>1</sup>H-NMR of a wash solution (Figure S11). In the FT-IR spectra, characteristic carboxylate peaks were observed at 1,600 cm<sup>-1</sup> in the CNC-COOH samples while a weak amine wag peak was observed at 850 cm<sup>-1</sup> in the CNC-NH<sub>2</sub> samples. While the amine wag peak has a high signal to noise ratio and cannot alone justify the presence of surface amines, later zeta potential measurements (Table 1) confirm that the CNCs functionalized by epichlorohydrinmediated amination have a positive surface charge which is consistent with the presence of amine groups on the CNC surface. For CNC-COOH samples, conductometric titrations indicated the presence of 900-1,300 mmol/kg carboxylate groups (Figure S9), providing further validation that the materials were successfully functionalized. AFM studies of the modified CNCs (Figure S10) confirmed that the dimensions of the CNCs did not change significantly during chemical functionalization, suggesting in tandem with WAXS (Table 1 and Figures S2-S6) that the conditions used for modification retained the crystallinity of the resulting materials. Finally, several of the isolated samples were dispersed in D<sub>2</sub>O and subsequently removed from the solution, and the D<sub>2</sub>O supernatants were analyzed by <sup>1</sup>H-NMR in reference to a 1 mg/mL maleic acid standard (Figure S11). The isolated and functionalized CNCs were free of contamination in the mmol contaminant/g CNC range, further justifying their use in later studies.

After confirming the chemical modification of the CNCs, electrophoretic light scattering experiments were conducted on a subset of the MxG-CNC samples to validate that the CNCs achieved the desired positive or negative charge modifications and further validate the chemical modification (Table 1 and Figure S12). Estimating the charge density on CNCs was critical to determine if and how charge properties alter biocompatibility in later analyses. Although electrophoretic light scattering is based off a spherical model, which is a poor description for the

long and rigid nanocrystals, the zeta potential ( $\zeta$ ) is directly proportional to the mobility ( $\mu$ ) as shown in (1); thus, these data provide a qualitative assessment of the surface charge.<sup>54</sup> MxG-CNCs were dispersed by brief ultrasonication in pH = 7 deionized water at a concentration of 1 mg/mL, passed through a 10  $\mu$ m filter to ensure the complete removal of large aggregates, and immediately analyzed. As expected, TEMPO oxidation imparted a strongly negative charge to the surface of CNCs at pH = 7 (-52.9±3.8 mV) while amination imparted a positive surface charge at pH = 7 (23.7±7.4 mV). Sulfated CNCs bore a comparable or slightly greater negative charge than the unfunctionalized CNCs, which is expected on account of the relatively low density of negatively charged sulfate half-ester moieties.<sup>55, 56</sup> Upon successfully completing characterization of the CNC samples, biological activity could be assayed.

$$\zeta = \frac{3\eta\mu}{2\varepsilon f\kappa R_h}$$

Source	Length	<b>Crystallinity Index</b>	Zeta Potential
t-CNC-OSO <sub>3</sub> -	820±400 nm	87%	-27.4±1.1 mV
MxG-CNC-OSO <sub>3</sub> -	120±40 nm	86%	-19.0±1.3 mV
MxG-CNC-OH	190±60 nm	88%	-16.3±0.4 mV
$MxG$ -CNC-OH $_{(ls)}$	200±80 nm	90%	-17.7±3.2 mV
c-CNC-OSO <sub>3</sub> -	90±20 nm	88%	-16.3±0.3 mV
w-CNC-OSO <sub>3</sub> -(ls)	110±40 nm	85%	-26.2±1.6 mV
<i>MxG</i> -CNC-COOH	N/A	86%	-52.9±3.4 mV
MxG-CNC-NH <sub>2</sub>	N/A	85%	23.7±7.4 mV

**Table 1:** Characterization of CNCs was conducted to evaluate length, crystallinity, and surface charge. The length of the CNCs was calculated for each of the samples using AFM peak height measurements or TEM images in the case of CNC-OH samples. Crystallinity index was calculated by obtaining WAXS spectra of all samples and using peak deconvolution to identify contributions from each of the four major cellulose  $1\beta$  crystalline peaks (101,  $10\overline{i}$ , 021, and 002) as well as the amorphous contribution to the spectrum. Finally, electrophoretic light scattering was used to

determine the zeta potential of CNC samples. CNC solutions were dispersed at 1 mg/mL by ultrasonication, and zeta potentials were obtained at 1 V and calculated using the linear polymer model (1) at pH=7 in water.

Endotoxin decontamination of samples. One challenge with studying the biological response of different CNCs is the possibility that the CNCs contain chemical or biological contaminants which can skew results and complicate data interpretation. Perhaps the most ubiquitous of these contaminants is bacterial endotoxin, a lipopolysaccharide which composes the outer membrane of gram-negative bacteria and induces cytotoxic responses by mTLR4 activation at trace concentrations (< 1 ng/mL).<sup>52</sup> Owing to its abundant presence in nature and amphiphilic nature, bacterial endotoxin previously has been found to adsorb strongly to nanoparticles, including CNCs.<sup>57</sup> The United States Pharmacopiea has reported an acceptable limit of 20 EU/device for medical devices, where EU is a measurement of the activity of endotoxin present in a sample.<sup>58</sup> Preliminary *in-vitro* assays with the CNCs indicated the presence of low-level immune activation and cytotoxicity that was suspected to result from such contamination; as such, methods to identify the presence and subsequently remove endotoxin from the CNC surface were explored.

Quantifying the presence of endotoxin on nanoparticle surfaces poses a unique challenge on account of the interaction of nanoparticles with common endotoxin test reagents.<sup>59, 60</sup> For example, LAL gel clot assay is a common semi-quantitative readout of endotoxin presence which is dependent on the interaction of the coagulin protein with lipopolysaccharide endotoxins to generate clotting. Many nanoparticle samples interact with coagulin, resulting in aberrant clotting and false positive results.<sup>59</sup> Other methods, such as the rabbit pyrogen test, are expensive and impractical for early-stage biocompatibility screening.<sup>60</sup> As such, the HEK mTLR4 cell line was used to quantify the presence of lipopolysaccharide endotoxins, where mTLR4 receptor activation by endotoxins result in the secretion of alkaline phosphatase (SEAP) which can be detected

colorimetrically by phosphatase detection reagents. Initial results indicated that *MxG*-CNC-COOH (and other samples) used directly without further purification did show some presence of endotoxin (Figure 3), albeit at relatively low levels. Nonetheless, it was decided to develop a cleaning procedure for all the CNCs to reduce any potential complications of endotoxin contamination.

Previous studies have reported the removal of endotoxin by treating nanoparticulate formulations with heat, solvent, or radiation. 53, 59, 61-63 Most commonly, samples are treated with dry heat or autoclave at 175-250 °C for several hours to induce decomposition of the lipopolysaccharide – this approach has proven successful for silicon, titanium, zirconium, and cobalt nanoparticles, as well as alginate-based biomaterials. 61, 62 Other studies have reported that extensive washing with ethanol, acetone, or strong acid removes endotoxin from titanium nanoparticles.<sup>63</sup> While these approaches have been successfully implemented in many cases, the low degradation temperature (approximately 130 °C), poor tolerance for strong acid, and negligible solubility in organic solvents of CNCs provided a unique challenge to remove endotoxin without damaging the CNCs. As such, a procedure using aqueous washes in tandem with ultrasonic treatment was developed based on inspiration from the medical device literature to clean the CNCs. 64 The CNCs were dispersed in endotoxin-free DI water, probe ultrasonicated for 5 min at 25% power (3 s on/off cycles), and then centrifugated to sediment the CNCs. The supernatant was then decanted and the procedure repeated for a total of three washes. The samples were then freeze dried, weighed and dispersed in endotoxin-free water for further use. This procedure afforded ca. 70 wt.% yield of CNCs and could be conducted in about one hour, providing a rapid and simple method to obtain clean samples for biological testing.

Using the described endotoxin removal procedure, all the CNC samples were cleaned and found to have endotoxin levels < 5 EU/mL when incubated at concentrations of 10-100  $\mu$ g/mL

with the HEK mTLR4 reporter cell line (Figure 3). Having successfully validated a reliable method to remove endotoxin from the samples, the ability of the CNC samples to activate the immune system in future experiments could be assayed.

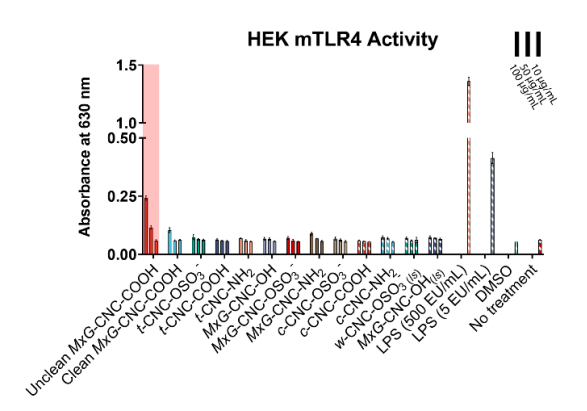


Figure 3: Endotoxin removal from CNC samples was validated using the HEK mTLR4 reporter assay (n=3/group). CNC samples were washed three times with endotoxin-free dH<sub>2</sub>O by subsequent sonication and ultracentrifugation. The cleaned samples were freeze dried, redissolved in endotoxin-free dH<sub>2</sub>O, and incubated with cells at 10-100 μg/mL overnight. HEK mTLR4 activity was indicated using HEK-Blue Detection Medium (InvivoGen), and absorbance was quantified at 620 nm. LPS was used as positive control, and an uncleaned sample (far left in red) with low-level endotoxin contamination is shown as a reference. Error bars indicate standard deviation.

*In-vitro* biocompatibility of CNCs. After successfully cleaning the samples, *in-vitro* biocompatibility of all the CNC samples was assayed. Given that CNCs isolated with hydrochloric or sulfuric acid hydrolysis, as well as those which have been further functionalized to achieve different charges or physicochemical properties, have been used in biological studies, <sup>20-28</sup> it was critical to establish a baseline for how different physicochemical parameters (such as charge and particle size) would affect the previously reported biocompatibility of CNCs. <sup>33-37</sup> As an initial test of cytotoxic activity induced by the CNCs with different sources, lengths, and charges, the RAW-Blue macrophage cell line was employed. Cells were incubated with 10-100 μg/mL of CNCs for

24 h, and an MTT assay was used as a colorimetric readout of mitochondrial activity to determine cytotoxicity. No changes in cytotoxicity were observed (Figure 4A), validating that altering source or charge of the CNCs had no bearing on cytotoxicity *in-vitro*. It is perhaps a little surprising that the positively charged CNCs did not induce cytotoxicity, as other cationic polymers such as poly(ethyleneimine) have been shown previously to induce apoptosis *in-vitro*. 65 As such, similar experiments were conducted using an alternative cytotoxicity assay which measures lactate dehydrogenase (LDH) activity. Again, no cytotoxicity was observed using the CNCs from various sources and charges, validating that the CNCs prepared for these studies did not activate cell death pathways under the conditions studied on account of their length or surface functionality (Figure S13). These results corroborated the prior experiments which suggested that CNCs are not cytotoxic regardless of the source or the charge *in-vitro*; however, it must be cautioned that other functionalization chemistry, such as those which include a longer linker, different pKa, or greater charge density, might influence cytotoxicity in the case of positively charged CNCs. Moreover, no significant differences between CNCs produced on a small scale or larger, commercially viable scale were observed, indicating that after the above cleaning procedure the method of isolation did not alter cytotoxicity of CNCs in-vitro.

After conducting the initial cytotoxicity assessments, immune activity of the 12 CNC samples was assayed. Previous studies have shown that many polymers, such as polystyrene or polycaprolactone, can induce nonspecific inflammation *in-vitro* as measured using RAW-Blue NF-κB activity.<sup>66, 67</sup> It is hypothesized that this nonspecific activation might arise from various physicochemical interactions of the polymers with innate immune cells; as such, it was important to assess whether different CNCs that vary in charge or particle size induce differential immune responses *in-vitro*. RAW-Blue cells have a SEAP reporter coupled to the NF-κB signal

transduction pathway which provides a broad readout of immune activation. CNCs were incubated with RAW-Blue cells for 24 h, and then the supernatant was collected and assayed using QuantiBlue detection reagent. No NF-κB signaling was induced by the CNCs with different lengths or charges (Figure 4B). IL-6 and TNF-α ELISAs were also conducted on supernatants as a secondary readout of immune activation. Low levels of TNF-α production were observed in most samples, indicating inflammation from cell damage independent of the NF-κB signaling pathway, while IL-6 was not induced (Figure S14-S15). Taken together, these results suggest that source/size or charge of the CNCs do not induce significant immune activation *in-vitro*.

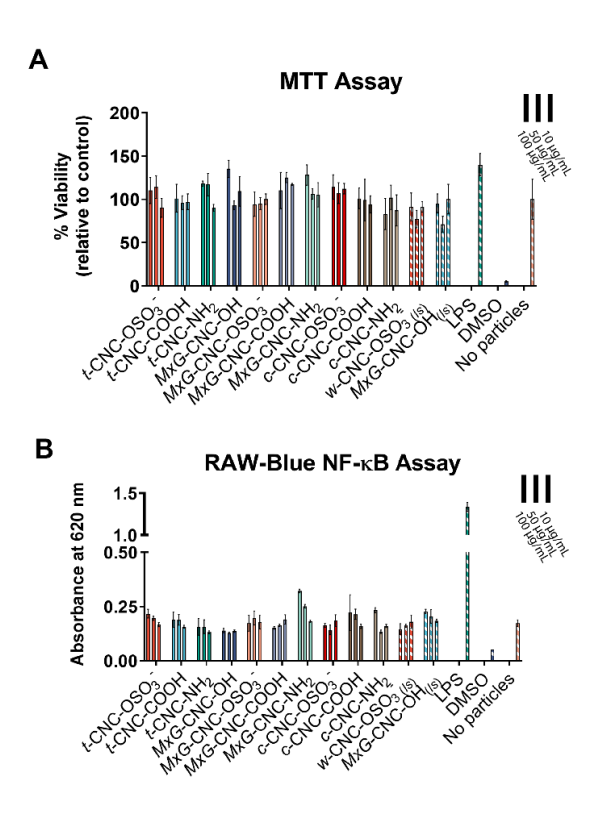


**Figure 4:** *In-vitro* assays assessing biocompatibility of the prepared CNCs (n=3/group). CNCs were incubated with the RAW-Blue macrophage cell line at 10-100 μg/mL for 24 h and (A) immune system activity and (B) cytotoxicity were assayed using RAW-Blue and MTT Assays, respectively. No aberrant immune system activity or cytotoxicity were observed using CNCs from any source or functionalization. Error bars indicate standard deviation.

Though the CNCs appeared to induce minimal immune activation or cytotoxicity *in-vitro*, an additional possibility was that CNCs could precipitate from cell culture media and disrupt cellular division. To test this hypothesis, a BrdU ELISA using RAW macrophages (the parent cell line of RAW-Blue macrophages) was conducted on a subset of the CNC samples to measure the rate of proliferation during incubation with the CNCs. BrdU is a thymidine analog which can be incorporated into host DNA to measure the rate of cell division. CNCs were incubated with the RAW macrophages for 12 h, and then BrdU-containing media was added for an additional 12 h to measure division using an anti-BrdU antibody ELISA. Again, no differences were observed (Figure S16). During the analyses, however, the presence of large aggregates in the *MxG*-CNC-OH samples were observed using a light microscope (Figure S17). Given these results, it was hypothesized that aggregation could damage tissue and result in systemic inflammation *in-vivo*, inspiring us to conduct an *in-vivo* biocompatibility assay in mice to test this possibility.

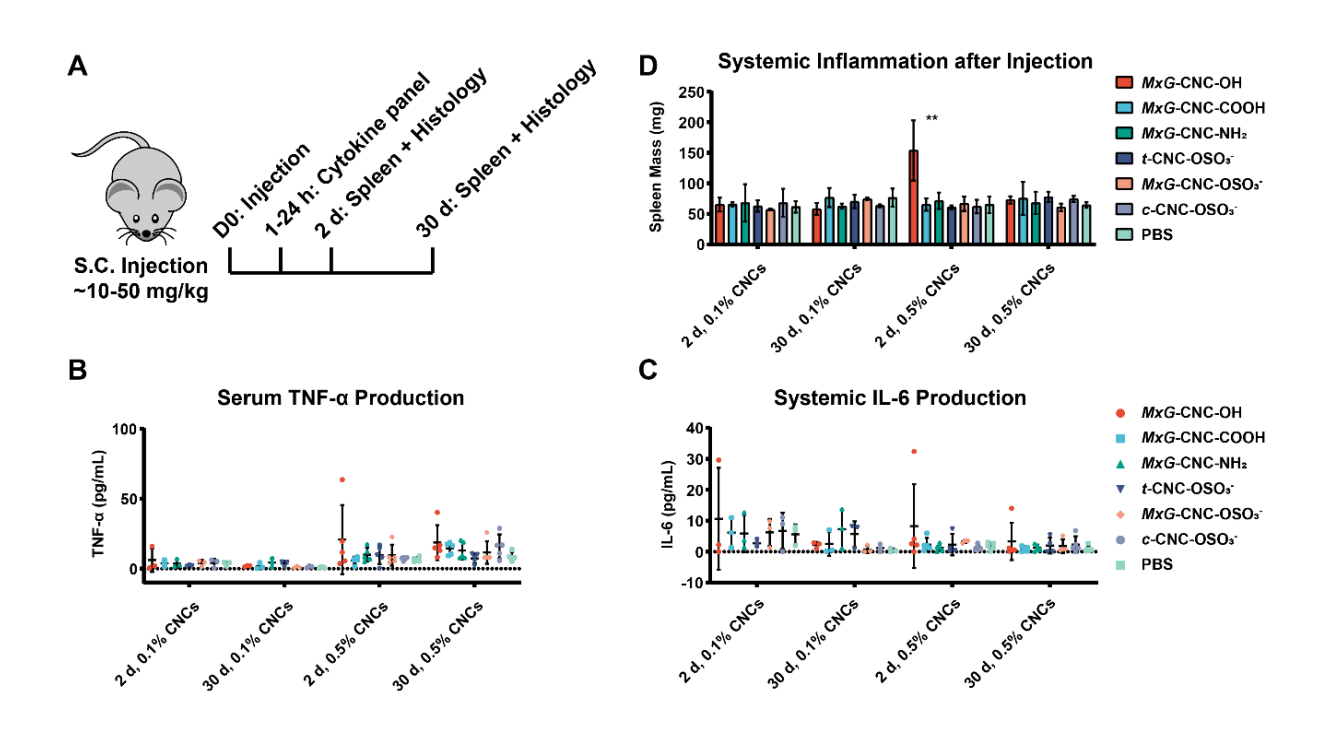


**Figure 5:** A) *In-vivo* experimental design to test inflammation induced by the CNCs (n=3-5/group). No changes in B) TNF- $\alpha$  or C) IL-6 were observed in the CNC samples at either concentration or timepoint analyzed. D) Mice injected with 0.5% *MxG*-CNC-OH had significant splenomegaly after 2 d, suggesting an acute immune response toward the CNCs. Error bars indicate standard deviation. Significant differences between treatments were analyzed by two-way ANOVA with residual multiple comparisons testing. \*\* = p < 0.01

**In-vivo biocompatibility of CNCs.** Having replicated and expanded upon previous invitro work demonstrating the biocompatibility of CNCs, an in-vivo experiment was designed using a subset of the CNCs to assay how size and charge would alter the acute inflammatory response towards CNCs in a mouse model. Given that CNCs in *in-vivo* applications have often been administered through subcutaneous routes of administration, 14, 26 six types of CNCs were injected subcutaneously (t-CNC-OSO<sub>3</sub>-, MxG-CNC-OSO<sub>3</sub>-, c-CNC-OSO<sub>3</sub>-, MxG-CNC-OH, MxG-CNC-COOH, and MxG-CNC-NH<sub>2</sub>), and the local and systemic immune response was assayed after 2 or 30 d. Two concentrations of CNCs were selected, 0.1% and 0.5%, as these concentrations were observed to be above and below the concentration threshold for dispersibility of the unfunctionalized (MxG-CNC-OH) samples. Using these two concentrations, experiments were conducted to evaluate if the effect of aggregation on in-vivo tissue compatibility of the CNCs could be assayed. Mice were injected subcutaneously in the right flank with 300 µL of the prescribed CNC solutions (corresponding to clinically relevant doses of approximately 10 and 50 mg/kg of CNCs), and the systemic immune response was assayed over 2-30 d using acute cytokine production (measured by ELISA), spleen mass, and hematoxylin and eosin staining of tissue from the injection site (Figure 5A). These outputs would afford a better understanding of systemic inflammation incurred by CNCs which could not be evaluated in-vitro.

As a measure of tissue damage and innate immune stimulation incurred by the CNCs, cytokine production was assayed in the serum after injection of the CNC samples. Immunotoxic nanoparticles induce secretion of cytokines into the bloodstream within hours of injection which can invoke a sickness response *in-vivo*.<sup>67, 68</sup> Thus, three pro-inflammatory cytokines (IL-6, TNF-α, and IFN-γ) were analyzed in the serum 1 and 24 h after injection. No significant difference in cytokine production was observed, indicating that the CNCs did not invoke acute serum toxicity at the timepoints analyzed (Figure 5B-C and Figure S18). These results corroborate the earlier *in-vitro* studies using the RAW-Blue cell line and suggest low systemic immunotoxicity of CNCs.

Tissue histology and spleen mass were then measured as indicators of local and systemic pro-inflammatory immune responses, respectively. While cytokine production provides temporal information about the acute inflammatory environment in response to CNCs, histology provides spatial information correlating inflammatory responses to tissue damage incurred by the CNCs. Additionally, spleen mass provides information about the systemic immune response to tissue damage at the site of injection. Mice were sacrificed after 2 or 30 d, and spleens were immediately weighed. In mice dosed with a 0.5% CNC solution, the unfunctionalized MxG-CNC-OH samples induced significant splenomegaly 2 d after injection (Figure 5D). This suggests the production of lymphocytes as an immune response was mounted, which is critical for proper wound healing in response to tissue damage. Further imaging of the injection site post-mortem revealed concurrent inflammation in the subcutaneous tissue of the mice injected with 0.5% MxG-CNC-OH after 2 d (Figure S19). The subcutaneous tissue was then dissected, fixed, and stained with hematoxylin and eosin. Staining revealed neutrophil infiltration and the presence of large CNC aggregates (> 50 μm) in tissue from the site of injection of mice injected with 0.5% MxG-CNC-OH after 2 d (Figure 6). No aggregates were observed in CNC-NH<sub>2</sub>, CNC-COOH, or CNC-OSO<sub>3</sub><sup>-</sup> samples at either timepoint, while limited neutrophil infiltration was observed in some samples (Figure 6 and Figure S20). Given that unfunctionalized CNC-OH are significantly more hydrophobic than CNCs containing amines, carboxylates, or sulfate half-esters, these results suggest that unfunctionalized CNCs have a higher aggregation propensity in tissue which can result in a systemic inflammatory response. Altogether, these results indicate that charged CNCs are nonimmunogenic and therefore viable for use in further biological experiments, while uncharged CNCs can generate undesirable inflammation at high concentrations which can result in tissue damage and sickness response.

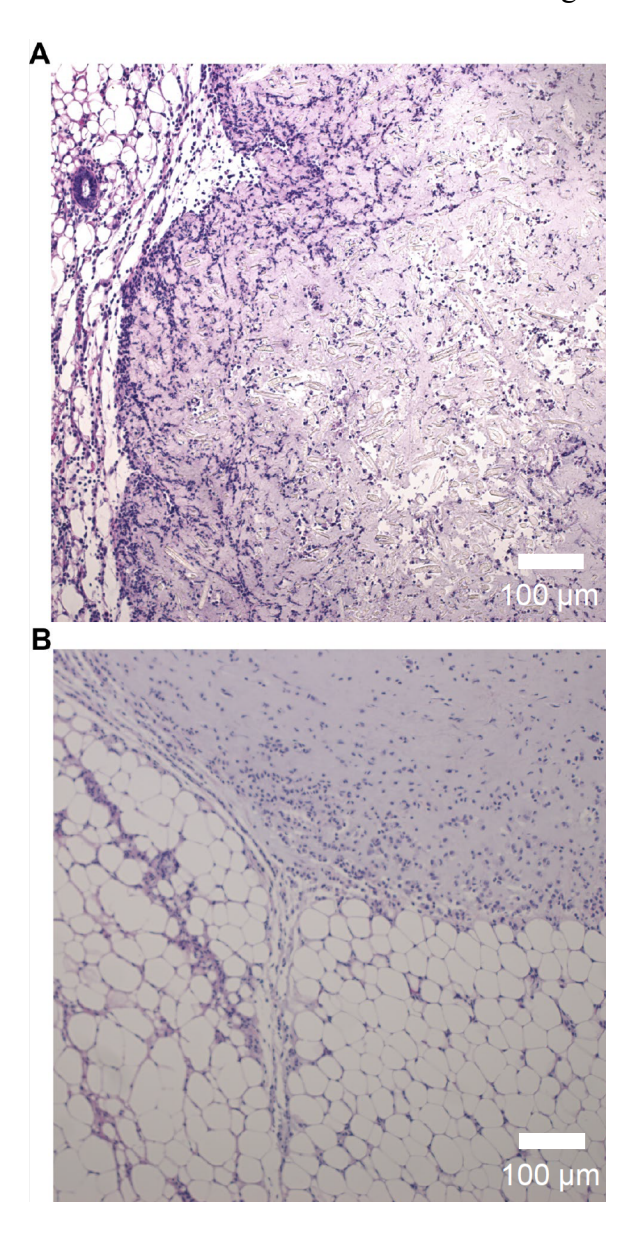


**Figure 6:** Hematoxylin and eosin staining of tissue collected from the injection site of uncharged A) *MxG*-CNC-OH and negatively charged B) *MxG*-CNC-COOH 2 d after injection. Significant neutrophil infiltration and presence of crystallite aggregates was observed in the *MxG*-CNC-OH samples suggesting a pro-inflammatory immune response.

# Conclusion

Reported herein is the *in-vitro* and *in-vivo* biocompatibility studies of CNCs from various biosources and with different surface charges. The CNCs were isolated, functionalized, and characterized from three biosources and obtained from two large-scale producers to yield a series of CNCs with a variety of lengths, charges, and isolation conditions. A simple procedure to remove endotoxin from the CNC surface was developed to allow decontamination prior to their use in biological systems. This procedure was replicated with all CNC samples, and the HEK mTLR4 reporter cell line was used to validate the removal of endotoxin from all samples. Given the increased use of CNCs in biological systems, this low cost and rapid purification procedure should facilitate enhanced reproducibility and validity of results in later biological studies.

The biocompatibility of CNCs with different length, source, and charge was assessed *invitro* and *in-vivo*. Unfunctionalized CNCs prepared through hydrochloric acid hydrolysis were observed to aggregate both in cell culture and in the tissue, resulting in acute systemic inflammation when injected subcutaneously in a murine model. Meanwhile, charged CNCs (achieved through surface modification to place amines, carboxylates, or sulfate half-ester moieties on the CNC surface) did not induce cytotoxicity or systemic inflammation *in-vitro* or *in-vivo*. These results suggest that CNCs functionalized with positive or negative charges are more appropriate for use in biomaterial tissue scaffold composites and hydrogels than unfunctionalized CNCs. Previous reports have indicated that CNCs remain in the tissue for several months after injection.<sup>26</sup> Understanding how CNCs interact with this tissue as a biomaterial scaffold degrades

or as CNCs leach from the scaffold is critical to the design principles for new biomaterial systems that utilize such nanomaterials.

While these results provide initial information on the biocompatibility of the CNCs studied, it will be critical to better understand how these materials interact with tissue both acutely and chronically. Future work must be conducted to evaluate long term interactions between CNCs and subcutaneous tissue, to study how different functionalization methods alter immune responses, to determine effects of CNCs administered through different routes of injection, and to learn if similar trends persist in higher order animals. Nonetheless, these results suggest that charged CNCs are compatible with biological tissue and have potential to be used in future biomedical applications.

# **Description of the Supporting Information Material**

The following files are available free of charge:

Additional methods, detailed characterization of CNCs including FT-IR, WAXS spectra, <sup>1</sup>H-NMR, TGA, and AFM, LDH assay results, IL-6 and TNF-α ELISA assay results, BrdU assay results, visualization of aggregates in *in-vitro* cell culture, additional *in-vivo* results.

#### **Author Contributions**

A.M.W., A.P.E-K., and S.J.R. conceived the study. A.M.W., N.M, Y.Z, and C.C. synthesized and characterized CNCs. A.M.W. conducted *in-vitro* and *in-vivo* experiments. A.M.W., A.P.E-K., and S.J.R. wrote the manuscript. All authors have given approval to the final version of the manuscript.

#### **Conflict of Interest Statement**

S.J.R. has an active patent (US10000578B2) on the production of cellulose nanocrystals from *Miscanthus x Giganteus*. A.M.W, N.M., Y.Z., C.C., and A.P.E-K. declare no competing interest.

# Acknowledgements

A.M.W. acknowledges financial support through an NIH Chemistry-Biology Interface training grant (T32 GM008720). C.C. acknowledges financial support through the Swiss National Science Foundation (SNSF) (P2FRP2\_181437). N.M., Y.Z., C.C., and S.J.R. acknowledge the National Science Foundation (NSF) Center for Sustainable Polymers (CSP) (CHE-1901635) for partial support of this work. A.P.E.-K. acknowledges the partial support of NIH (U01AI124286) and DTRA (1-18-1-0052). The authors thank the University of Chicago veterinary technicians for exceptional animal care, Dr. Mark Lingen for assistance with histopathological analysis, Dr. Phil Griffin for DLS measurements, and the beamline scientists at Argonne National Lab for technical support. We also acknowledge the MRSEC Shared User Facilities (NSF DMR-2011854), Soft Matter Characterization Facility, X-Ray Research Facility, NMR facility, and Human Tissue Resource Center at the University of Chicago for support.

# References

- 1. Habibi, Y.; Lucia, L. A.; Rojas, O. J., Cellulose nanocrystals: chemistry, self-assembly, and applications. *Chem Rev* **2010**, 110 (6), 3479-500.
- 2. Elazzouzi-Hafraoui, S.; Nishiyama, Y.; Putaux, J. L.; Heux, L.; Dubreuil, F.; Rochas, C., The shape and size distribution of crystalline nanoparticles prepared by acid hydrolysis of native cellulose. *Biomacromolecules* **2008**, 9 (1), 57-65.
- 3. Cheng, M.; Qin, Z.; Liu, Y.; Qin, Y.; Li, T.; Chen, L.; Zhu, M., Efficient extraction of

- carboxylated spherical cellulose nanocrystals with narrow distribution through hydrolysis of lyocell fibers by using ammonium persulfate as an oxidant. *J. Mater. Chem. A* **2014**, 2 (1), 251-258.
- 4. Calvino, C.; Macke, N.; Kato, R.; Rowan, S. J., Development, processing and applications of bio-sourced cellulose nanocrystal composites. *Prog Polym Sci* **2020**, 103, 101221.
- 5. Mariano, M.; El Kissi, N.; Dufresne, A., Cellulose nanocrystals and related nanocomposites:

  Review of some properties and challenges. *J Polym Sci Polym Phys* **2014**, 52 (12), 791-806.
- 6. Tang, J.; Sisler, J.; Grishkewich, N.; Tam, K. C., Functionalization of cellulose nanocrystals for advanced applications. *J Colloid Interface Sci* **2017**, 494, 397-409.
- Wohlhauser, S.; Delepierre, G.; Labet, M.; Morandi, G.; Thielemans, W.; Weder, C.; Zoppe,
   J. O., Grafting Polymers from Cellulose Nanocrystals: Synthesis, Properties, and
   Applications. *Macromolecules* 2018, 51 (16), 6157-6189.
- 8. Charreau, H.; Cavallo, E.; Foresti, M. L., Patents involving nanocellulose: Analysis of their evolution since 2010. *Carbohyd Polym* **2020**, 237, 116039.
- 9. Lin, N.; Dufresne, A., Nanocellulose in biomedicine: Current status and future prospect. *Eur Polym J* **2014**, 59, 302-325.
- 10. Domingues, R. M.; Gomes, M. E.; Reis, R. L., The potential of cellulose nanocrystals in tissue engineering strategies. *Biomacromolecules* **2014**, 15 (7), 2327-2346.
- 11. Guo, J.; Liu, D.; Filpponen, I.; Johansson, L. S.; Malho, J. M.; Quraishi, S.; Liebner, F.; Santos, H. A.; Rojas, O. J., Photoluminescent Hybrids of Cellulose Nanocrystals and Carbon Quantum Dots as Cytocompatible Probes for in Vitro Bioimaging. *Biomacromolecules* 2017, 18 (7), 2045-2055.

- 12. Imlimthan, S.; Otaru, S.; Keinanen, O.; Correia, A.; Lintinen, K.; Santos, H. A.; Airaksinen, A. J.; Kostiainen, M. A.; Sarparanta, M., Radiolabeled Molecular Imaging Probes for the In Vivo Evaluation of Cellulose Nanocrystals for Biomedical Applications. *Biomacromolecules* 2019, 20 (2), 674-683.
- 13. Kumar, A.; Negi, Y. S.; Choudhary, V.; Bhardwaj, N. K., Microstructural and mechanical properties of porous biocomposite scaffolds based on polyvinyl alcohol, nanohydroxyapatite and cellulose nanocrystals. *Cellulose* **2014**, 21 (5), 3409-3426.
- 14. Li, W.; Lan, Y.; Guo, R.; Zhang, Y.; Xue, W.; Zhang, Y., In vitro and in vivo evaluation of a novel collagen/cellulose nanocrystals scaffold for achieving the sustained release of basic fibroblast growth factor. *J Biomater Appl* **2015**, 29 (6), 882-893.
- 15. Zhang, H.; Feng, M.; Chen, S.; Shi, W.; Wang, X., Incorporation of lysozyme into cellulose nanocrystals stabilized beta-chitosan nanoparticles with enhanced antibacterial activity. *Carbohydr Polym* **2020**, 236, 115974.
- 16. Nguyen, J. K.; Park, D. J.; Skousen, J. L.; Hess-Dunning, A. E.; Tyler, D. J.; Rowan, S. J.; Weder, C.; Capadona, J. R., Mechanically-compliant intracortical implants reduce the neuroinflammatory response. *J Neural Eng* 2014, 11 (5), 056014.
- 17. Nguyen, J. K.; Jorfi, M.; Buchanan, K. L.; Park, D. J.; Foster, E. J.; Tyler, D. J.; Rowan, S. J.; Weder, C.; Capadona, J. R., Influence of resveratrol release on the tissue response to mechanically adaptive cortical implants. *Acta Biomater* **2016**, 29, 81-93.
- 18. Capadona, J. R.; Tyler, D. J.; Zorman, C. A.; Rowan, S. J.; Weder, C., Mechanically adaptive nanocomposites for neural interfacing. *MRS Bulletin* **2012**, 37 (6), 581-589.
- 19. Salimi, S.; Sotudeh-Gharebagh, R.; Zarghami, R.; Chan, S. Y.; Yuen, K. H., Production of

- Nanocellulose and Its Applications in Drug Delivery: A Critical Review. *ACS Sustain Chem Eng* **2019**, 7 (19), 15800-15827.
- 20. Dong, S.; Cho, H. J.; Lee, Y. W.; Roman, M., Synthesis and cellular uptake of folic acid-conjugated cellulose nanocrystals for cancer targeting. *Biomacromolecules* **2014**, 15 (5), 1560-1567.
- 21. Mangalam, A. P.; Simonsen, J.; Benight, A. S., Cellulose/DNA hybrid nanomaterials. *Biomacromolecules* **2009**, 10 (3), 497-504.
- 22. Wang, H.; He, J.; Zhang, M.; Tam, K. C.; Ni, P., A new pathway towards polymer modified cellulose nanocrystals via a "grafting onto" process for drug delivery. *Polym Chem* **2015**, 6 (23), 4206-4209.
- 23. Akhlaghi, S. P.; Berry, R. C.; Tam, K. C., Surface modification of cellulose nanocrystal with chitosan oligosaccharide for drug delivery applications. *Cellulose* **2013**, 20 (4), 1747-1764.
- 24. Abouhmad, A.; Dishisha, T.; Amin, M. A.; Hatti-Kaul, R., Immobilization to Positively

  Charged Cellulose Nanocrystals Enhances the Antibacterial Activity and Stability of Hen

  Egg White and T4 Lysozyme. *Biomacromolecules* **2017**, 18 (5), 1600-1608.
- 25. Dong, S.; Roman, M., Fluorescently labeled cellulose nanocrystals for bioimaging applications. *J Am Chem Soc* **2007**, 129 (45), 13810-13811.
- 26. De France, K. J.; Badv, M.; Dorogin, J.; Siebers, E.; Panchal, V.; Babi, M.; Moran-Mirabal, J.; Lawlor, M.; Cranston, E. D.; Hoare, T., Tissue Response and Biodistribution of Injectable Cellulose Nanocrystal Composite Hydrogels. ACS Biomater Sci Eng 2019, 5 (5), 2235-2246.
- 27. Lin, N.; Geze, A.; Wouessidjewe, D.; Huang, J.; Dufresne, A., Biocompatible Double-

- Membrane Hydrogels from Cationic Cellulose Nanocrystals and Anionic Alginate as Complexing Drugs Codelivery. *ACS Appl Mater Interfaces* **2016**, 8 (11), 6880-6889.
- 28. Ndong Ntoutoume, G. M.; Grassot, V.; Bregier, F.; Chabanais, J.; Petit, J. M.; Granet, R.; Sol, V., PEI-cellulose nanocrystal hybrids as efficient siRNA delivery agents-Synthesis, physicochemical characterization and in vitro evaluation. *Carbohydr Polym* 2017, 164, 258-267.
- 29. Naahidi, S.; Jafari, M.; Edalat, F.; Raymond, K.; Khademhosseini, A.; Chen, P., Biocompatibility of engineered nanoparticles for drug delivery. *J Control Release* 2013, 166 (2), 182-194.
- 30. Poland, C. A.; Duffin, R.; Kinloch, I.; Maynard, A.; Wallace, W. A.; Seaton, A.; Stone, V.; Brown, S.; Macnee, W.; Donaldson, K., Carbon nanotubes introduced into the abdominal cavity of mice show asbestos-like pathogenicity in a pilot study. *Nat Nanotechnol* **2008**, 3 (7), 423-428.
- 31. Sayes, C. M.; Liang, F.; Hudson, J. L.; Mendez, J.; Guo, W.; Beach, J. M.; Moore, V. C.; Doyle, C. D.; West, J. L.; Billups, W. E.; Ausman, K. D.; Colvin, V. L., Functionalization density dependence of single-walled carbon nanotubes cytotoxicity in vitro. *Toxicol Lett* **2006**, 161 (2), 135-142.
- 32. Castranova, V.; Porter, D.; Millecchia, L.; Ma, J. Y.; Hubbs, A. F.; Teass, A., Effect of inhaled crystalline silica in a rat model: time course of pulmonary reactions. *Mol Cell Biochem* 2002, 234-235 (1-2), 177-184.
- 33. Yanamala, N.; Farcas, M. T.; Hatfield, M. K.; Kisin, E. R.; Kagan, V. E.; Geraci, C. L.;

- Shvedova, A. A., In Vivo Evaluation of the Pulmonary Toxicity of Cellulose Nanocrystals: A Renewable and Sustainable Nanomaterial of the Future. *ACS Sustain Chem Eng* **2014**, 2 (7), 1691-1698.
- 34. Endes, C.; Mueller, S.; Kinnear, C.; Vanhecke, D.; Foster, E. J.; Petri-Fink, A.; Weder, C.; Clift, M. J.; Rothen-Rutishauser, B., Fate of cellulose nanocrystal aerosols deposited on the lung cell surface in vitro. *Biomacromolecules* **2015**, 16 (4), 1267-1275.
- 35. Dong, S.; Hirani, A. A.; Colacino, K. R.; Lee, Y. W.; Roman, M., Cytotoxicity and Cellular Uptake of Cellulose Nanocrystals. *Nano LIFE* **2012**, 2 (3), 1241006.
- 36. Mahmoud, K. A.; Mena, J. A.; Male, K. B.; Hrapovic, S.; Kamen, A.; Luong, J. H., Effect of surface charge on the cellular uptake and cytotoxicity of fluorescent labeled cellulose nanocrystals. *ACS Appl Mater Interfaces* **2010**, 2 (10), 2924-2932.
- 37. Sunasee, R.; Araoye, E.; Pyram, D.; Hemraz, U. D.; Boluk, Y.; Ckless, K., Cellulose nanocrystal cationic derivative induces NLRP3 inflammasome-dependent IL-1beta secretion associated with mitochondrial ROS production. *Biochem Biophys Rep* **2015**, 4, 1-9.
- 38. Harper, B. J.; Clendaniel, A.; Sinche, F.; Way, D.; Hughes, M.; Schardt, J.; Simonsen, J.; Stefaniak, A. B.; Harper, S. L., Impacts of chemical modification on the toxicity of diverse nanocellulose materials to developing zebrafish. *Cellulose* **2016**, 23 (3), 1763-1775.
- 39. Labet, M.; Thielemans, W., Improving the reproducibility of chemical reactions on the surface of cellulose nanocrystals: ROP of  $\varepsilon$ -caprolactone as a case study. *Cellulose* **2011**, 18 (3), 607-617.
- 40. Colombo, L.; Zoia, L.; Violatto, M. B.; Previdi, S.; Talamini, L.; Sitia, L.; Nicotra, F.;

- Orlandi, M.; Salmona, M.; Recordati, C.; Bigini, P.; La Ferla, B., Organ Distribution and Bone Tropism of Cellulose Nanocrystals in Living Mice. *Biomacromolecules* **2015**, 16 (9), 2862-2871.
- 41. Ventura, C.; Pinto, F.; Lourenço, A. F.; Ferreira, P. J. T.; Louro, H.; Silva, M. J., On the toxicity of cellulose nanocrystals and nanofibrils in animal and cellular models. *Cellulose* **2020**, *27* (10), 5509-5544.
- 42. Dagnon, K. L.; Shanmuganathan, K.; Weder, C.; Rowan, S. J., Water-Triggered Modulus

  Changes of Cellulose Nanofiber Nanocomposites with Hydrophobic Polymer Matrices. *Macromolecules* **2012**, 45 (11), 4707-4715.
- 43. Cudjoe, E.; Hunsen, M.; Xue, Z.; Way, A. E.; Barrios, E.; Olson, R. A.; Hore, M. J.; Rowan,
  S. J., Miscanthus Giganteus: A commercially viable sustainable source of cellulose nanocrystals. *Carbohydr Polym* 2017, 155, 230-241.
- 44. Capadona, J. R.; Shanmuganathan, K.; Trittschuh, S.; Seidel, S.; Rowan, S. J.; Weder, C., Polymer nanocomposites with nanowhiskers isolated from microcrystalline cellulose. *Biomacromolecules* **2009**, 10 (4), 712-716.
- 45. Habibi, Y.; Chanzy, H.; Vignon, M. R., TEMPO-mediated surface oxidation of cellulose whiskers. *Cellulose* **2006**, 13 (6), 679-687.
- 46. Olkowski, A. A.; Laarveld, B.; Arrison, N. Catalytic Biomass Conversion. U.S. Patent 2017/0016179A1, January 19 2017.
- 47. McAlpine, S.; Nakoneshny, J. Production of Crystalline Cellulose. W.O. Patent PCT/CA2017/050096, August 3 2017.
- 48. Dahl, E. K.; Krumdick, G.; Pupek, K. Methods of Producing Cellulose Nanocrystals. U.S. Patent 2019/0367704 A1, December 5 2019.

- 49. Rowan, S. J.; Hunsen, M.; Way, A. Method for Production of Cellulose Nanocrystals from Miscanthus Giganteus and Composites Therefrom. U.S. Patent 10000578 B2, June 19, 2018.
- 50. Park, S.; Baker, J. O.; Himmel, M. E.; Parilla, P. A.; Johnson, D. K., Cellulose crystallinity index: measurement techniques and their impact on interpreting cellulase performance. *Biotechnol Biofuels* **2010**, 3, 10.
- 51. French, A. D., Idealized powder diffraction patterns for cellulose polymorphs. *Cellulose* **2013**, 21 (2), 885-896.
- 52. Li, Y.; Boraschi, D., Endotoxin contamination: a key element in the interpretation of nanosafety studies. *Nanomedicine* **2016**, 11 (3), 269-287.
- 53. Roman, M.; Winter, W. T., Effect of sulfate groups from sulfuric acid hydrolysis on the thermal degradation behavior of bacterial cellulose. *Biomacromolecules* **2004**, 5 (5), 1671-1677.
- 54. Delgado, A. V.; González-Caballero, F.; Hunter, R. J.; Koopal, L. K.; Lyklema, J., Measurement and Interpretation of Electrokinetic Phenomena (IUPAC Technical Report). Pure Appl Chem 2005, 77 (10), 1753-1805.
- 55. Araki, J.; Wada, M.; Kuga, S.; Okano, T., Influence of surface charge on viscosity behavior of cellulose microcrystal suspension. *J Wood Sci* **1999**, 45 (3), 258-261.
- 56. Kargarzadeh, H.; Ahmad, I.; Abdullah, I.; Dufresne, A.; Zainudin, S. Y.; Sheltami, R. M., Effects of hydrolysis conditions on the morphology, crystallinity, and thermal stability of cellulose nanocrystals extracted from kenaf bast fibers. *Cellulose* **2012**, *19* (3), 855-866.
- 57. Nordli, H. R.; Chinga-Carrasco, G.; Rokstad, A. M.; Pukstad, B., Producing ultrapure wood cellulose nanofibrils and evaluating the cytotoxicity using human skin cells. *Carbohydr Polym* **2016**, *150*, 65-73.

- 58. U.S. Pharmacopiea and National Foundry (USP31–NF26). Transfusion and Infusion Assemblies and Similar Medical Devices, U.S. Pharmacopeial Convention, Rockville, MD, Rockville, MD, 2011.
- 59. Smulders, S.; Kaiser, J. P.; Zuin, S.; Van Landuyt, K. L.; Golanski, L.; Vanoirbeek, J.; Wick, P.; Hoet, P. H., Contamination of nanoparticles by endotoxin: evaluation of different test methods. *Part Fibre Toxicol* **2012**, 9, 41.
- 60. Dobrovolskaia, M. A.; Neun, B. W.; Clogston, J. D.; Ding, H.; Ljubimova, J.; McNeil, S. E., Ambiguities in applying traditional Limulus amebocyte lysate tests to quantify endotoxin in nanoparticle formulations. *Nanomedicine* **2010**, 5 (4), 555-562.
- 61. Chansoria, P.; Narayanan, L. K.; Wood, M.; Alvarado, C.; Lin, A.; Shirwaiker, R. A., Effects of Autoclaving, EtOH, and UV Sterilization on the Chemical, Mechanical, Printability, and Biocompatibility Characteristics of Alginate. *ACS Biomater Sci Eng* **2020**, 6 (9), 5191-5201.
- 62. Marilena, L.; Antonietta, M. G.; Graziana, S.; Paola, Q.; Lucia, M.; Emanuela, M.; Diana, B., Innate defense functions of macrophages can be biased by nano-sized ceramic and metallic particles. *Eur Cytokine Netw* **2004**, 15 (4), 339-346.
- 63. Schwab, L. P.; Xing, Z.; Hasty, K. A.; Smith, R. A., Titanium particles and surface-bound LPS activate different pathways in IC-21 macrophages. *J Biomed Mater Res B Appl Biomater* **2006**, 79 (1), 66-73.
- 64. Tarafa, P. J.; Williams, E.; Panvelker, S.; Zhang, J.; Matthews, M. A., Removing Endotoxin from Metallic Biomaterials with Compressed Carbon Dioxide-Based Mixtures. *J Supercrit Fluids* **2011**, *55* (3), 1052-1058.
- 65. Moghimi, S. M.; Symonds, P.; Murray, J. C.; Hunter, A. C.; Debska, G.; Szewczyk, A., A

- two-stage poly(ethylenimine)-mediated cytotoxicity: implications for gene transfer/therapy. *Mol Ther* **2005**, *11* (6), 990-995.
- 66. Moser, B. A.; Steinhardt, R. C.; Esser-Kahn, A. P., Surface Coating of Nanoparticles Reduces

  Background Inflammatory Activity while Increasing Particle Uptake and Delivery. *ACS Biomater Sci Eng* **2017**, 3 (2), 206-213.
- 67. Maiti, S.; Manna, S.; Shen, J.; Esser-Kahn, A. P.; Du, W., Mitigation of Hydrophobicity-Induced Immunotoxicity by Sugar Poly(orthoesters). *J Am Chem Soc* **2019**, 141 (11), 4510-4514.
- 68. Semete, B.; Booysen, L. I.; Kalombo, L.; Venter, J. D.; Katata, L.; Ramalapa, B.; Verschoor, J. A.; Swai, H., In vivo uptake and acute immune response to orally administered chitosan and PEG coated PLGA nanoparticles. *Toxicol Appl Pharmacol* **2010**, 249 (2), 158-165.

# **Table of Contents Graphic**

